Geophysical Research Letters

RESEARCH LETTER
10.1029/2022GL102249

Rapid Development of Systematic ENSO-Related Seasonal Forecast Errors

J. D. Beverley[1,2], M. Newman[2], and A. Hoell[2]

[1]Cooperative Institute for Research in Environmental Sciences (CIRES), University of Colorado Boulder, Boulder, CO, USA, [2]NOAA Physical Sciences Laboratory, Boulder, CO, USA

Key Points:

- Seasonal forecast models have systematic sea surface temperature and precipitation errors related to long-standing El Niño-Southern Oscillation (ENSO) simulation errors
- In 11 operational models, predicted ENSO anomalies typically extend too far westward and their maxima decay too slowly in the east
- These errors develop rapidly, within 1–2 weeks after initialization, to become more dependent upon verification month than upon lead time

Supporting Information:

Supporting Information may be found in the online version of this article.

Correspondence to:

J. D. Beverley,
jonathan.beverley@noaa.gov

Citation:

Beverley, J. D., Newman, M., & Hoell, A. (2023). Rapid development of systematic ENSO-related seasonal forecast errors. *Geophysical Research Letters*, *50*, e2022GL102249. https://doi.org/10.1029/2022GL102249

Received 22 NOV 2022
Accepted 30 APR 2023

Abstract Climate models exhibit known systematic errors in their representation of the El Niño-Southern Oscillation (ENSO). In this study, we show that such simulation errors are largely present in tropical seasonal prediction, even for short lead times. Regressing monthly forecast errors from 11 different operational models upon the observed ENSO state, we find that predicted ENSO-related sea surface temperature anomalies (of either sign) for winter/spring are significantly extended or shifted to the west and are also too persistent during the ENSO decay phase, both common climate model errors. There are also corresponding precipitation forecast errors, most notably a robust westward shift of the ENSO-related precipitation dipole that may impact predictions of extratropical teleconnections. These ENSO-related errors develop within days after initialization regardless of month, including significant errors appearing in anomalous surface trade winds, and saturate so rapidly that they primarily depend upon the seasonal cycle rather than lead time.

Plain Language Summary El Niño-Southern Oscillation (ENSO; the slowly varying sea surface temperature [SST] anomalies in the tropical Pacific) has an important influence on global climate and can provide a valuable source of skill for seasonal tropical and extratropical forecasts. However, models contain biases in their simulation of ENSO-related SSTs, including extending the SST anomalies associated with ENSO events too far to the west in the tropical Pacific. We find that these errors develop within days of the forecast start time, are much more closely tied to the seasonal cycle than forecast lead time (the length of time after the forecast start date), and they seem to develop first in the atmosphere before subsequently influencing SST and precipitation errors. As precipitation in the tropics is closely tied to SSTs, these SST errors result in a westward shift of tropical precipitation relative to observations, which has important implications for tropical and extratropical seasonal forecast skill through driving errors in remote atmospheric waves.

1. Introduction

El Niño-Southern Oscillation (ENSO) is a key driver of seasonal climate across the globe, making it a primary focus for numerical modeling centers. However, most climate model simulations exhibit systematic ENSO errors (Bellenger et al., 2014), including a tendency to extend ENSO equatorial Pacific sea surface temperature (SST) anomalies (of either sign) too far westward, with a related westward shift in anomalous precipitation, and ENSO events that generally decay too slowly during late winter and spring following their peak in the eastern equatorial Pacific. Most models also have mean biases in their tropical Pacific SSTs, such as a "cold tongue bias" where eastern equatorial Pacific climatological SSTs are colder than observed (Li & Xie, 2014), as well as errors in the trend of the equatorial zonal SST gradient (Lee et al., 2022; Seager et al., 2019, 2022). These simulation errors have existed for many model generations, at least as early as CMIP3 (Joseph & Nigam, 2006) and continuing through CMIP6 (Capotondi et al., 2020; R. Chen et al., 2020; H.-C. Chen et al., 2021; Deser et al., 2018).

Similar models are also used by operational centers to make seasonal climate predictions, raising the possibility that these model errors also impact forecast skill. For example, while many seasonal forecast models show high skill predicting ENSO variations in the central Pacific (e.g., within the Niño3.4 region, L'Heureux et al., 2020), their skill for the remainder of the tropical Pacific is lower, especially in the western tropical Pacific (Imada et al., 2015; Newman & Sardeshmukh, 2017; Wu et al., 2022; Zhang et al., 2017). Model predictions also have errors in their temporal evolution of ENSO events, for example, during springtime, when models overpredict Niño3.4 SST tendencies (Tippett et al., 2020), as well as tropical Pacific SST trend errors similar to those found in climate models (L'Heureux et al., 2022). Such ENSO forecast errors will likely impact extratropical model skill,

through inducing errors in Rossby wave propagation (see e.g., Figure A4 of Deser et al., 2018), so understanding them could lead to improvements in subseasonal-to-seasonal prediction.

In this study, we investigate systematic ENSO forecast errors in eleven state-of-the-art operational prediction models, to diagnose how their development might relate to erroneous climate model ENSO states. We identify ENSO-related tropical forecast errors by regressing them against the observed Niño3.4 index, characterizing their spatial structure and temporal evolution as a function of both forecast lead and seasonal cycle. The remainder of the paper is arranged as follows. Section 2 introduces details of the models and our analysis methods. Our results, presented in Section 3, reveal that the error develops very rapidly and is strongly tied to the seasonal cycle, suggesting that climate model errors have a pronounced impact on seasonal forecasts. Some further implications are discussed in Section 4.

2. Data and Methods

We use multi-decade hindcasts from 11 different operational seasonal forecast models (Batté et al., 2021; Delworth et al., 2020; Fröhlich et al., 2021; Gualdi et al., 2020; Hirahara et al., 2023; Johnson et al., 2019; Lin et al., 2020; MacLachlan et al., 2015; Molod et al., 2020; Saha et al., 2014—see Table S1 in Supporting Information S1 for a detailed list). These models use either first-of-the-month initializations or lagged ensembles, although we find the results largely insensitive to initialization method. We focus on hindcasts made prior to and during the peak of ENSO, initialized in months ranging from July–February. We use monthly mean SST, precipitation and 10 m zonal wind from all models and daily means (averaged to pentad values) of these variables for models for which data was available to us (SEAS5, GCFS2.1, CanCM4i, and SPS3.5). Ensemble means are used since our focus is on systematic ENSO errors.

Hindcasts are verified against the ECMWF fifth generation reanalysis (ERA5, Hersbach et al., 2020). Hindcasts are first bias-corrected by removing the lead-dependent seasonally-varying mean bias for each model (Figure S1 in Supporting Information S1 shows an example of DJF SST biases for October initialization hindcasts). Multi-model ensemble means (hereafter MMM) are computed by averaging ensemble means from multiple models; for example, MMM forecast error variance is computed by determining the forecast error variance for each model's hindcast data set, then computing the mean of the hindcast variances. Analysis of individual models uses all available years, while MMM quantities use the common years (1994–2016), but results are essentially unchanged regardless.

Free-running climate model ENSO errors (i.e., those within long climate model simulations) are often determined by comparing model and observed regression patterns based on their respective Niño indices. To instead diagnose errors in model predictions of observed ENSO states, and to allow for clean comparison of these errors across forecast models, we define the "ENSO-related" error at each gridpoint from the regression of forecast errors (i.e., forecast minus verification) against the observed (i.e., verification) Niño3.4 indices obtained from area-averaging the ERA5 SST anomaly within the region bounded by 170°W–120°W, 5°N–5°S (Barnston et al., 1997):

$$\text{Forecast error} \equiv y_f^{\tau} - y_{obs} = m^{\tau} N_{3.4,\,obs} + \epsilon \tag{1}$$

where y_f^{τ} is the forecast variable at lead time τ, y_{obs} is the observed variable at the same verification time, m^{τ} is the regression coefficient (the "ENSO-related error"), $N_{3.4,\,obs}$ is the observed Niño3.4 index and ϵ is the regression error. Note that this is the same as taking the difference of the regression coefficients calculated by regressing the forecast and observed anomalies on the observed Niño3.4 index (m_f^{τ} and m_{obs}):

$$y_f^{\tau} = m_f^{\tau} N_{3.4,\,obs} + \epsilon_f \tag{2}$$

$$y_{obs} = m_{obs} N_{3.4,\,obs} + \epsilon_{obs} \tag{3}$$

$$m^{\tau} = m_f^{\tau} - m_{obs} \tag{4}$$

Our main points are unchanged if ENSO is defined using either the Niño3 or Niño4 indices, or by regressing against the Niño3.4 index of the initialization, rather than verification.

To determine if the regressions are unduly influenced by individual ENSO events, given the limited length of hindcasts (between 23 and 36 years), we conduct a Monte Carlo test where 1,000 artificial time series are created

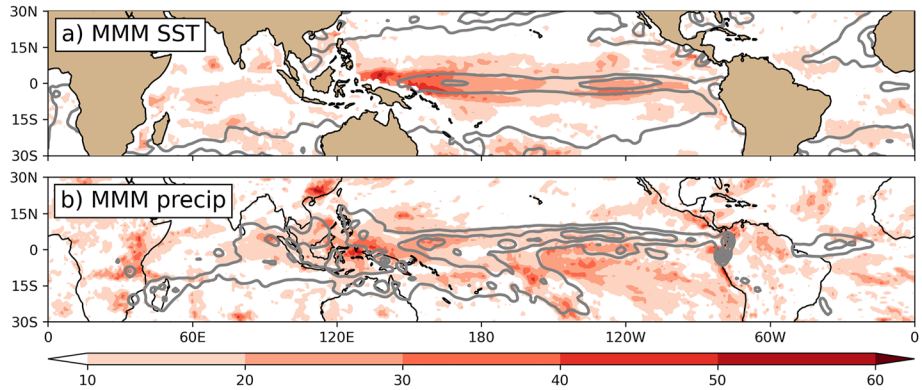

Figure 1. Shading shows the December–January–February MMM percentage of error variance explained by the observed Niño3.4 index for (a) sea surface temperature (SST) and (b) precipitation. Gray contours show the variance of the model error in each variable (contours at [0.2, 0.4, 0.6, … K^2] for SST and [4, 8, 12, … $mm^2\ d^{-2}$] for precipitation).

by randomly selecting the relevant number of years from each hindcast set, with replacement. For example, with the 36 year hindcast period of SEAS5, this yields 1,000 time series of 36 years. Regressions are computed from each time series to create a distribution of regression coefficients, and then the actual regression coefficient is labeled significant if it falls above or below the 97.5th or 2.5th percentile of this distribution, respectively.

3. Results

3.1. Monthly Mean ENSO-Related Errors

To first illustrate ENSO's importance to tropical forecast error, Figure 1 shows the MMM forecast error variance for DJF-seasonal mean hindcasts initialized in October, for SST and precipitation. Shading shows the percentage of error variance explained by the observed Niño3.4 index, calculated by correlating the model error (model minus observations) with the observed Niño3.4 index, squaring it, then multiplying by 100. ENSO explains between 10% and 20% or more of the SST forecast error variance in the equatorial strip spanning the Pacific Ocean. In the western equatorial Pacific, where hindcast error variance is relatively high, ENSO explains almost half of the error variance (and greater than 70% for some models; Figure S2 in Supporting Information S1), even though forecast error variance also includes loss of predictability due to initial condition uncertainty (e.g., Newman & Sardeshmukh, 2017) and potentially other sources of systematic error.

Precipitation error variance has a maximum in the western tropical Pacific, with high values extending across the tropical Pacific north of the equator. ENSO explains slightly less error variance for precipitation than SST, with more spatial heterogeneity, but its impact still exceeds 40% in the western tropical Pacific (Figure S3 in Supporting Information S1 shows individual models). Overall, ENSO is strongly linked to both SST and precipitation errors throughout the tropical Pacific, particularly in the western equatorial Pacific, as well as to errors in remote ENSO-impacted regions including Peru and sub-Saharan Africa.

ENSO-related SST errors across the 11 models for October-initialized DJF seasonal mean hindcasts share substantial commonalities that can be characterized in a few ways; four representative examples are shown in Figure 2 (all 11 models are shown in Figure S4 in Supporting Information S1), but the features shown in the MMM of these four (Figure 2e) are also seen in the 11-models MMM (Figure 2f). Virtually all models show some positive west Pacific error, indicative of a westward extension of the predicted (same sign) SST anomaly. (Note that positive regression values mean the error is in the same direction as the ENSO phase; i.e., errors are shaded for the El Niño phase, so for La Niña the sign is reversed.) Seven models have significant positive errors in the eastern tropical Pacific (e.g., CanCM4i, GEM5-NEMO, Figures 2b and 2c), consistent with model simulations that overestimate ENSO amplitude, which may also be related to seasonal cycle errors. Some models (e.g., SPEAR, GCFS2.1, CFSv2, Figure 2d and Figure S4 in Supporting Information S1) have negative errors in the central–eastern Pacific, corresponding to underpredicted ENSO amplitudes there. Depending upon the precise longitudinal positioning of this error and the positive western Pacific error, the predicted ENSO SST anomaly is either shifted (rather than extended) westward or weakened. In the Indian Ocean, where El Niño typically drives

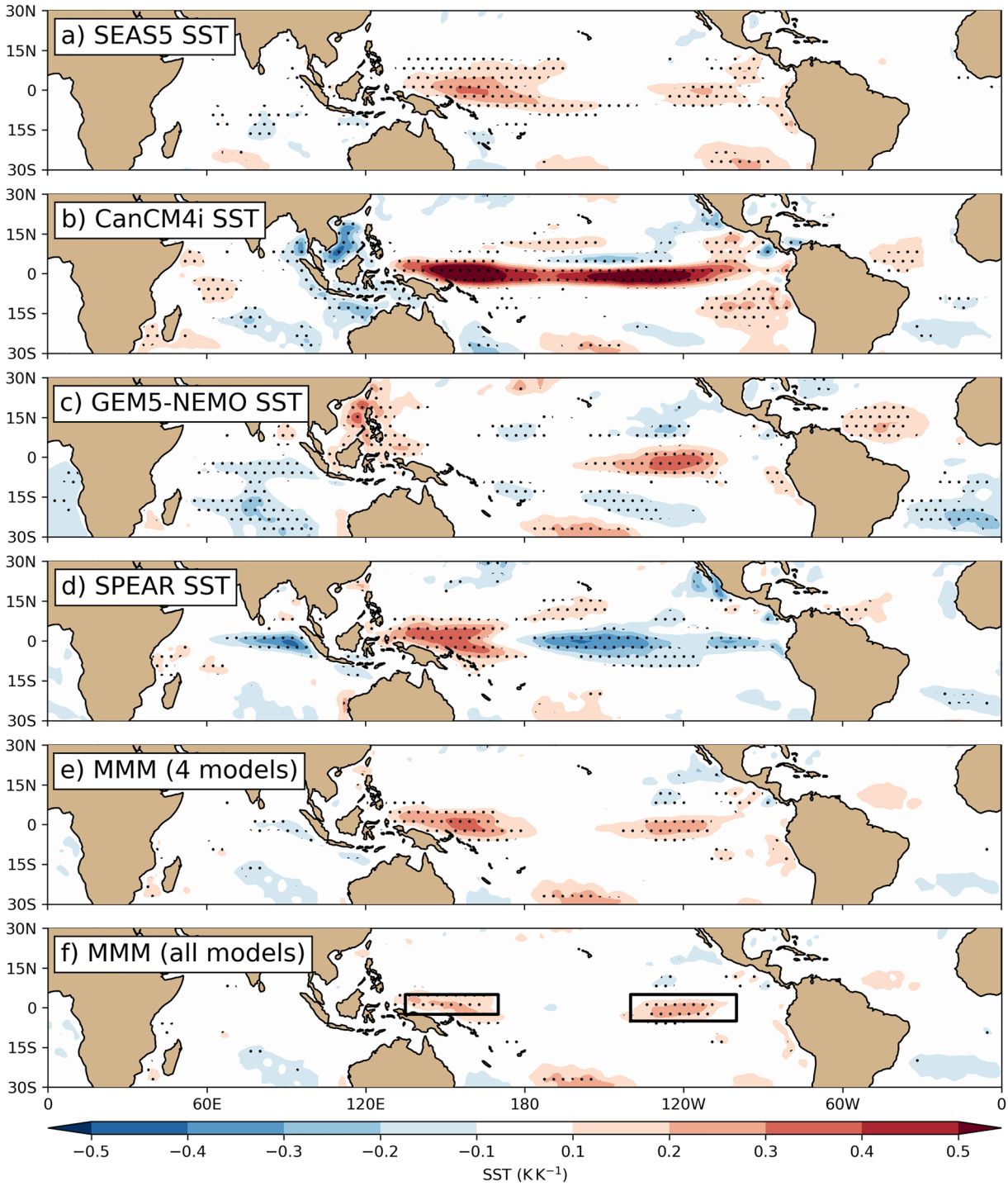

Figure 2. December–January–February El Niño–Southern Oscillation (ENSO)-related sea surface temperature error for forecasts initialized in October for (a–d) four representative seasonal forecast models, (e) the multi-model mean of these four models and (f) the multi-model mean of all 11 models. Stippling indicates significance based on 1000 Monte Carlo samples (see Section 2). Maps for all individual models are in Figure S4 in Supporting Information S1. Boxes on (f) are used in subsequent analysis.

a basin-wide warming during winter/spring (e.g., Alexander et al., 2002), the ENSO-related SST error bears a resemblance to the positive phase of the Indian Ocean Dipole (IOD, Saji et al., 1999), which is characterized by warmer SSTs in the western Indian Ocean and cooler SSTs in the eastern Indian Ocean, possibly due to ENSO's westward shift.

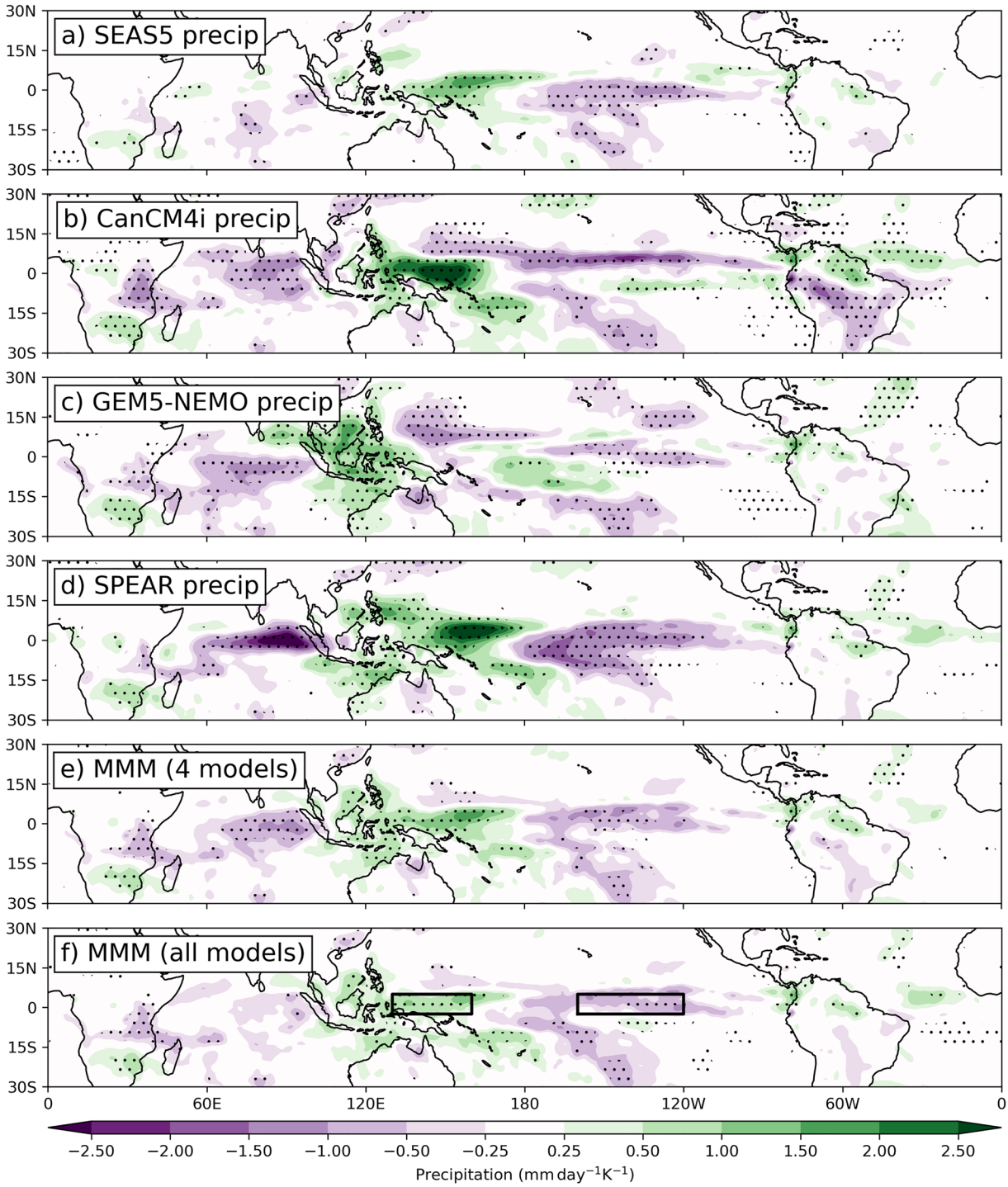

Figure 3. December–January–February El Niño–Southern Oscillation (ENSO)-related precipitation error for forecasts initialized in October for (a–d) four representative seasonal forecast models, (e) the multi-model mean of these four models and (f) the multi-model mean of all 11 models. Stippling indicates significance based on 1000 Monte Carlo samples (see Section 2). Maps for all individual models are in Figure S5 in Supporting Information S1. Boxes on (f) are used in subsequent analysis.

The ENSO-related precipitation hindcast error patterns are more consistent across models (Figure 3 and Figure S5 in Supporting Information S1), generally showing a dipole structure with positive (negative) values in the western (central) tropical Pacific, indicating a westward shift of the typical ENSO precipitation anomaly that is

evident in the MMMs (Figures 3e and 3f). This westward shift (occurring for ENSO anomalies of either sign) might impact extratropical seasonal forecast skill through inducing errors in Rossby wave propagation.

Although ENSO-related errors are particularly notable in the tropical Pacific, the erroneous westward shift of precipitation could correspond to a shift in the Walker circulation leading to errors in other tropical regions. Significant ENSO-related precipitation errors over Africa, consistent across the models, are the reverse of the canonical El Niño response (negative precipitation anomalies over southern Africa/positive anomalies over eastern equatorial Africa). Most models also show negative ENSO-related precipitation error over the Indian Ocean and consistent signals over parts of South America and the tropical Atlantic.

Similar error patterns are also obtained by instead determining warm-minus-cold composite errors based on Niño3.4. Moreover, comparing these to warm-plus-cold composite errors shows that the ENSO-related errors are mostly symmetric (equal and opposite) for ENSO phase (Figures S6 and S7 in Supporting Information S1). This linear relationship is also seen by plotting Niño3.4 against the hindcast errors within both the west and east Pacific (boxes on Figures 2f and 3f; Figure S8 in Supporting Information S1).

We next show how the ENSO-related errors for SST and precipitation vary primarily by verification month, with a weaker dependence upon lead time. In Figures 4a–4d, ENSO-related errors for the west and east Pacific boxes are shown as a function of forecast lead time (colors), with each symbol indicating a different initialization month. The variability of ENSO-related errors across individual models is shown with the gray dots.

For SST (Figures 4a and 4b), the ENSO-related error in the west Pacific peaks around September/October and January/February (soon after the typical ENSO event peak—though some individual models peak in April), while the east Pacific error peaks in April, consistent with model-simulated ENSO events decaying too slowly in spring. Note that while there is a relatively large spread for the individual models, the late winter/spring behavior of the east Pacific SST error is qualitatively consistent across virtually all the models. Also, while seasonality impacts both the regression and Niño3.4 amplitudes, the Niño3.4 index explains roughly 20%–40% of the SST error variance in the West Pacific and 20%–30% in the East Pacific every month (Figure S9 in Supporting Information S1).

The seasonal dependence of the ENSO-related precipitation errors (Figures 4c and 4d) is even more apparent, with MMM errors peaking in February–April. Note that both regions move together through winter, so that the ENSO-related error in the precipitation dipole (i.e., the westward shift of predicted anomalous precipitation in Figure 3) intensifies through February. Variance explained is slightly lower than for SST, but still 10%–20% in the West Pacific and 20%–30% in the East Pacific, declining toward the spring (Figure S9 in Supporting Information S1).

Also noteworthy is that the ENSO-related error magnitude depends primarily on verification month, although there is some intensification with lead time (Figures 4a–4d), particularly for east Pacific SST and west Pacific precipitation, where the ENSO-related error has similar amplitude for a range of lead times for a given verification month; conversely, simulations with the same lead time but different verification month have relatively large range. For example, the western Pacific ENSO-related precipitation error for 1-month lead (red symbols on Figure 4c) varies between 0 and 1.25 mm d^{-1} K^{-1}. This is similar to the results of Barnston et al. (2019), who showed that NMME skill for the Niño3.4 index is lower for certain "target months" than others.

More generally, the patterns of ENSO-related error are more dependent upon verification month than lead time. For example, the pattern of the ENSO-related error for hindcasts verifying in February is very similar whether the hindcasts are initialized in October or December. This is also true for hindcasts verifying in other months. In contrast, error patterns of hindcasts initialized in different months but with the same lead time are quite dissimilar. While this is evident from visual inspection of the individual ENSO-related error patterns for SST and precipitation (Figures S10 and S11 in Supporting Information S1), we quantify it by computing pattern correlations between all error patterns (for different verification months and leads, for SST and precipitation) and a specified verification base month at 0-month lead. The average of these pattern correlations for four different base months (November–February), shown in Figures 4e and 4f, shows a pronounced maximum along the diagonal from lower-left to upper-right, indicating that the patterns of ENSO-related error for the same verification month are similar for any lead time. In contrast, error patterns for hindcasts with similar lead times but different verification months are less similar, indicated by the smaller correlation values in the columns/rows of Figures 4e and 4f.

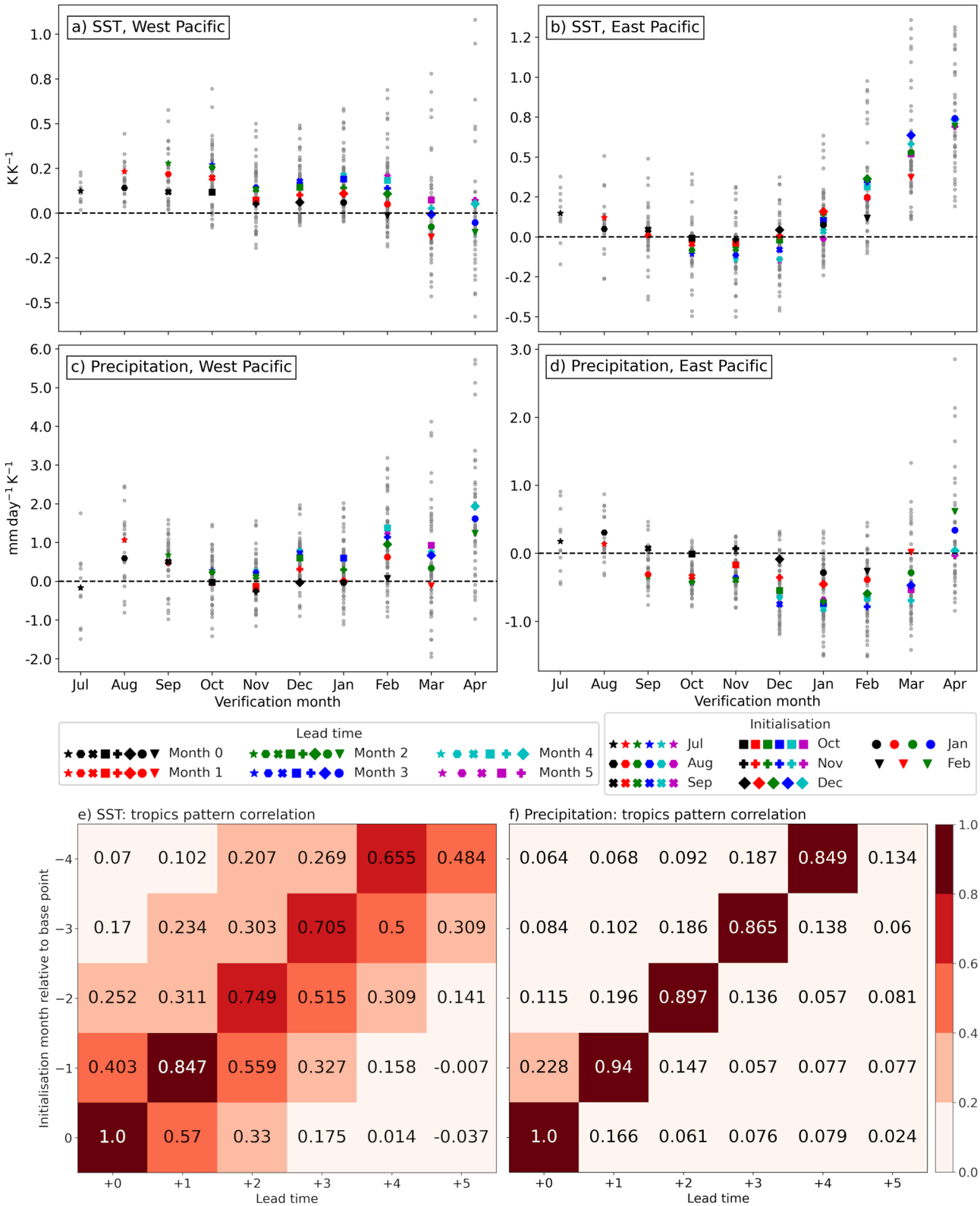

Figure 4. MMM El Niño–Southern Oscillation (ENSO)-related error for (a, b) sea surface temperature (SST) and (c, d) precipitation averaged over (a, c) the West Pacific and (b, d) the East Pacific regions shown in Figures 2f and 3f; note these are slightly different for SST and precipitation. Different colors represent different lead times (Month 0 being the first month of the hindcast); different symbols represent different initialization months. Gray dots indicate individual model simulations. (e) and (f) show the pattern correlations for tropical ENSO-related SST and precipitation errors averaged for four different base months as a function of lead time and initialization (see text).

However, correlation values off the diagonal do not decrease as readily for SST as they do for precipitation, as the spatial patterns of ENSO-related SST error show some dependence upon lead time.

3.2. Pentad-Averaged ENSO-Related Errors

We now examine how the ENSO-related errors evolve on a sub-monthly timescale. Figure 5 shows Hovmöller diagrams of the evolution of pentad-averaged ENSO-related error for SEAS5 hindcasts (October–January initializations), for SST (contours), precipitation (shading) and 10 m zonal wind (vectors—non-significant vectors are gray), averaged between 5°N and 5°S for longitudes extending from the Maritime Continent to South America. Results for other forecast models are in Figures S12–S14 in Supporting Information S1; these have differences in detail consistent with the results discussed earlier, but all share the same basic elements: a rapid initial development of ENSO-related errors and a strong seasonal modulation of those errors.

For all four SEAS5 initializations, statistically significant ENSO-related errors develop within the first hindcast pentad (i.e., Days 1–5 mean), generally starting with errors in SST and 10 m zonal wind in the western-central equatorial Pacific which persist in sign, if not always amplitude, throughout the hindcast. The positive west Pacific SST error amplifies more rapidly in the October initializations in SEAS5 and SPS3.5, but is similar across all initializations for GCFS2.1 and CanCM4i (Figure S15 in Supporting Information S1). The positive western tropical Pacific wind error corresponds to an easterly error for an El Niño event, implying a too-weak westerly wind anomaly and correspondingly weakened Bjerknes feedback, consistent with the positive west Pacific ENSO-related SST error. Westerly errors over the Maritime Continent result in an area of anomalous convergence leading to significant positive ENSO-related precipitation error over the western tropical Pacific. In addition, during late spring the positive ENSO-related SST error in the east Pacific intensifies before rapidly changing sign in mid-May (also seen in other models; Figures S12–S14 in Supporting Information S1). This is consistent with models overpredicting the springtime Niño3.4 SST tendency (or "excessive momentum") found by Tippett et al. (2020), suggesting that ENSO climate model error may be responsible for their result.

Error seasonality is also apparent when comparing these four initializations. For example, the positive eastern Pacific ENSO-related SST error takes nearly 4 months to develop from the October initialization, yet is visible only a few weeks after the January initialization. The significant western Pacific ENSO-related precipitation error first appears around March for all four initialization times and peaks at almost the same late-April date, along with the easterly 10 m wind error near the dateline. This is also true for west Pacific ENSO-related SST error for the other three models (Figure S15 in Supporting Information S1). This further emphasizes the dependence of the ENSO-related error on the seasonal cycle, more than on lead time.

4. Summary and Conclusions

Although ENSO is a key source of tropical and extratropical seasonal forecast skill, large systematic errors in its prediction remain, including a westward extension/shift of ENSO anomalies toward the western tropical Pacific and a too-slow decay of ENSO events, both of which were identified in the bias-corrected hindcasts in this study. These forecast errors develop rapidly, evolving to primarily depend upon the seasonal cycle, rather than lead time, after only about 1–2 months. This result is consistent with the view that the ENSO forecast anomalies transition quickly from nature's attractor to the climate model attractor and consequently the ENSO-related forecast error approaches the free-running climate model error (see Section 2). Both ENSO forecasts and their errors in initialized seasonal forecast systems may then be largely understood through investigation of the uninitialized model space (e.g., Ding et al., 2018).

While it is difficult to draw firm conclusions about the origin of these errors, some of our results suggest they occur first in the near-surface winds, which subsequently influence SST errors. This is slightly more obvious for GCFS2.1 and SPS3.5 (Figures S12 and S14 in Supporting Information S1), and when using daily rather than pentad averages (not shown). Note also that the initial development of the ENSO-related error occurs within days after forecast initialization, while the model and observed mean states are still reasonably close. Initialization shock could also be a contributing factor. To examine these questions further may require analysis of 6-hourly forecast data from more frequently issued hindcasts than used here.

ENSO has strong extratropical teleconnections via Rossby wave excitation driven by anomalous tropical divergence (Sardeshmukh & Hoskins, 1988), so the systematic error in ENSO precipitation anomalies should be

10.1029/2022GL102249

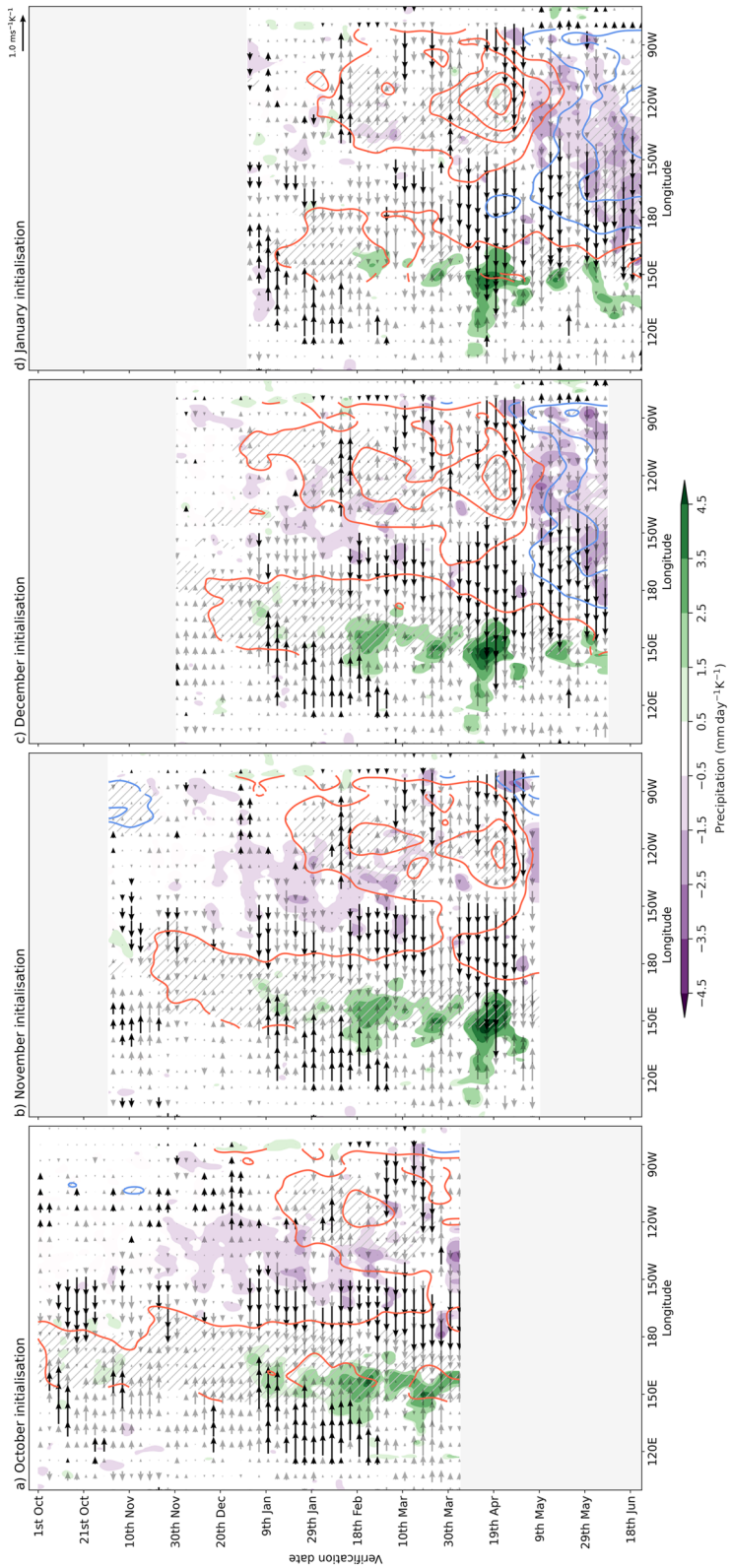

Figure 5. Hovmöller diagrams showing the evolution of pentad-averaged El Niño–Southern Oscillation (ENSO)-related error for SEAS5 October–January initializations for sea surface temperature (SST) (contours), precipitation (shading) and 10 m zonal wind (vectors) averaged between 5°N and 5°S. For precipitation, only significant values are plotted. Significant wind vectors are shown in black. Significance for SST is shown by the gray hatching. SST contours are every 0.2 K K^{-1}, including contours for −0.1 and 0.1 K K^{-1} (blue for negative, red for positive). Areas shaded gray are before the beginning or after the end of the hindcasts.

expected to impact extratropical seasonal forecast skill, although errors in the propagation pathway (e.g., the upper-level jet) can also contribute (Garfinkel et al., 2022; Williams et al., 2023). Complicating matters further is that ENSO's observed impact on the extratropics has a multivariate spatiotemporal dependence (e.g., Zhao et al., 2021), partly due to ENSO diversity (Capotondi et al., 2020), which also may not be entirely constrained by the limited observational record (e.g., Deser et al., 2018). Evaluating and diagnosing how ENSO's systematic errors impact extratropical skill will be the topic of a follow-up study.

Data Availability Statement

Monthly Copernicus seasonal forecast model data are available at https://doi.org/10.24381/cds.68dd14c3 and daily Copernicus seasonal forecast model data are available at https://doi.org/10.24381/cds.181d637e. ERA5 data can be downloaded at https://doi.org/10.24381/cds.f17050d7. NASA GEOS-S2S and GFDL-SPEAR hindcasts can be downloaded at http://iridl.ldeo.columbia.edu/SOURCES/.Models/.NMME/.NASA-GEOSS2S/.HINDCAST/.MONTHLY/ and http://iridl.ldeo.columbia.edu/SOURCES/.Models/.NMME/.GFDL-SPEAR/.HINDCAST/.MONTHLY/, respectively.

Acknowledgments
This work was partially supported by NOAA cooperative agreements NA17OAR4320101 and NA22OAR4320151 and the Famine Early Warning Systems Network. The authors wish to thank Michael Alexander for his helpful feedback. We are also grateful to the two anonymous reviewers for their constructive comments.

References

Alexander, M. A., Bladé, I., Newman, M., Lanzante, J. R., Lau, N.-C., & Scott, J. D. (2002). The atmospheric bridge: The influence of ENSO teleconnections on air–sea interaction over the global oceans. *Journal of Climate*, *15*(16), 2205–2231. https://doi.org/10.1175/1520-0442(2002)015<2205:tabtio>2.0.co;2

Barnston, A. G., Chelliah, M., & Goldenberg, S. B. (1997). Documentation of a highly ENSO-related SST region in the equatorial Pacific: Research note. *Atmosphere-Ocean*, *35*(3), 367–383. https://doi.org/10.1080/07055900.1997.9649597

Barnston, A. G., Tippett, M. K., Ranganathan, M., & L'Heureux, M. L. (2019). Deterministic skill of ENSO predictions from the North American multimodel ensemble. *Climate Dynamics*, *53*(12), 7215–7234. https://doi.org/10.1007/s00382-017-3603-3

Batté, L., Dorel, L., Ardilouze, C., & Guérémy, J. (2021). Documentation of the METEO-FRANCE seasonal forecasting system 8. Technical report.

Bellenger, H., Guilyardi, É., Leloup, J., Lengaigne, M., & Vialard, J. (2014). Enso representation in climate models: From CMIP3 to CMIP5. *Climate Dynamics*, *42*(7–8), 1999–2018. https://doi.org/10.1007/s00382-013-1783-z

Capotondi, A., Deser, C., Phillips, A., Okumura, Y., & Larson, S. (2020). ENSO and Pacific decadal variability in the Community Earth System Model version 2. *Journal of Advances in Modeling Earth Systems*, *12*(12), e2019MS002022. https://doi.org/10.1029/2019ms002022

Chen, H.-C., Fei, F.-J., Zhao, S., Wittenberg, A. T., & Xie, S. (2021). ENSO dynamics in the E3SM-1-0, CESM2, and GFDL-CM4 climate models. *Journal of Climate*, *34*(23), 9365–9384. https://doi.org/10.1175/JCLI-D-21-0355.1

Chen, R., Simpson, I. R., Deser, C., & Wang, B. (2020). Model biases in the simulation of the springtime North Pacific ENSO teleconnection. *Journal of Climate*, *33*(23), 9985–10002. https://doi.org/10.1175/jcli-d-19-1004.1

Delworth, T. L., Cooke, W. F., Adcroft, A., Bushuk, M., Chen, J.-H., Dunne, K. A., et al. (2020). SPEAR: The next generation GFDL modeling system for seasonal to multidecadal prediction and projection. *Journal of Advances in Modeling Earth Systems*, *12*(3), e2019MS001895. https://doi.org/10.1029/2019ms001895

Deser, C., Simpson, I. R., Phillips, A. S., & McKinnon, K. A. (2018). How well do we know ENSO's climate impacts over North America, and how do we evaluate models accordingly? *Journal of Climate*, *31*(13), 4991–5014. https://doi.org/10.1175/jcli-d-17-0783.1

Ding, H., Newman, M., Alexander, M. A., & Wittenberg, A. T. (2018). Skillful climate forecasts of the tropical Indo-Pacific Ocean using model-analogs. *Journal of Climate*, *31*(14), 5437–5459. https://doi.org/10.1175/jcli-d-17-0661.1

Fröhlich, K., Dobrynin, M., Isensee, K., Gessner, C., Paxian, A., Pohlmann, H., et al. (2021). The German climate forecast system: GCFS. *Journal of Advances in Modeling Earth Systems*, *13*(2), e2020MS002101. https://doi.org/10.1029/2020ms002101

Garfinkel, C. I., Chen, W., Li, Y., Schwartz, C., Yadav, P., & Domeisen, D. (2022). The winter North Pacific teleconnection in response to ENSO and the MJO in operational subseasonal forecasting models is too weak. *Journal of Climate*, *35*(24), 1–39. https://doi.org/10.1175/jcli-d-22-0179.1

Gualdi, S., Borrelli, A., Cantelli, A., Davoli, G., Mar Chavesmontero, M. D., Masina, S., et al. (2020). The new CMCC operational seasonal prediction system. CMCC Technial Note (RP0288). https://doi.org/10.25424/CMCC/SPS3.5

Hersbach, H., Bell, B., Berrisford, P., Hirahara, S., Horányi, A., Muñoz-Sabater, J., et al. (2020). The ERA5 global reanalysis. *Quarterly Journal of the Royal Meteorological Society*, *146*(730), 1999–2049. https://doi.org/10.1002/qj.3803

Hirahara, S., Kubo, Y., Yoshida, T., Komori, T., Chiba, J., Takakura, T., et al. (2023). Japan Meteorological Agency/Meteorological Research Institute Coupled Prediction System version 3 (JMA/MRI-CPS3). *Journal of the Meteorological Society of Japan*, *101*(2), 149–169. https://doi.org/10.2151/jmsj.2023-009

Imada, Y., Tatebe, H., Ishii, M., Chikamoto, Y., Mori, M., Arai, M., et al. (2015). Predictability of two types of El Niño assessed using an extended seasonal prediction system by MIROC. *Monthly Weather Review*, *143*(11), 4597–4617. https://doi.org/10.1175/mwr-d-15-0007.1

Johnson, S. J., Stockdale, T. N., Ferranti, L., Balmaseda, M. A., Molteni, F., Magnusson, L., et al. (2019). SEAS5: The new ECMWF seasonal forecast system. *Geoscientific Model Development*, *12*(3), 1087–1117. https://doi.org/10.5194/gmd-12-1087-2019

Joseph, R., & Nigam, S. (2006). ENSO evolution and teleconnections in IPCC's twentieth-century climate simulations: Realistic representation? *Journal of Climate*, *19*(17), 4360–4377. https://doi.org/10.1175/jcli3846.1

Lee, S., L'Heureux, M., Wittenberg, A. T., Seager, R., O'Gorman, P. A., & Johnson, N. C. (2022). On the future zonal contrasts of equatorial Pacific climate: Perspectives from Observations, Simulations, and Theories. *npj Climate and Atmospheric Science*, *5*(1), 82. https://doi.org/10.1038/s41612-022-00301-2

L'Heureux, M. L., Levine, A. F., Newman, M., Ganter, C., Luo, J.-J., Tippett, M. K., & Stockdale, T. N. (2020). ENSO prediction. In *El Niño Southern Oscillation in a changing climate* (pp. 227–246). Wiley Online Library.

L'Heureux, M. L., Tippett, M. K., & Wang, W. (2022). Prediction challenges from errors in tropical Pacific sea surface temperature trends. *Frontiers in Climate*, *27*, 837483. https://doi.org/10.3389/fclim.2022.837483

Li, G., & Xie, S.-P. (2014). Tropical biases in CMIP5 multimodel ensemble: The excessive equatorial Pacific cold tongue and double ITCZ problems. *Journal of Climate*, *27*(4), 1765–1780. https://doi.org/10.1175/jcli-d-13-00337.1

Lin, H., Merryfield, W. J., Muncaster, R., Smith, G. C., Markovic, M., Dupont, F., et al. (2020). The Canadian seasonal to interannual prediction system version 2 (CanSIPSv2). *Weather and Forecasting*, *35*(4), 1317–1343. https://doi.org/10.1175/waf-d-19-0259.1

MacLachlan, C., Arribas, A., Peterson, K. A., Maidens, A., Fereday, D., Scaife, A., et al. (2015). Global seasonal forecast system version 5 (GloSea5): A high-resolution seasonal forecast system. *Quarterly Journal of the Royal Meteorological Society*, *141*(689), 1072–1084. https://doi.org/10.1002/qj.2396

Molod, A., Hackert, E., Vikhliaev, Y., Zhao, B., Barahona, D., Vernieres, G., et al. (2020). GEOS-S2S version 2: The GMAO high-resolution coupled model and assimilation system for seasonal prediction. *Journal of Geophysical Research: Atmospheres*, *125*(5), e2019JD031767. https://doi.org/10.1029/2019jd031767

Newman, M., & Sardeshmukh, P. D. (2017). Are we near the predictability limit of tropical Indo-Pacific sea surface temperatures? *Geophysical Research Letters*, *44*(16), 8520–8529. https://doi.org/10.1002/2017gl074088

Saha, S., Moorthi, S., Wu, X., Wang, J., Nadiga, S., Tripp, P., et al. (2014). The NCEP climate forecast system version 2. *Journal of Climate*, *27*(6), 2185–2208. https://doi.org/10.1175/jcli-d-12-00823.1

Saji, N., Goswami, B. N., Vinayachandran, P., & Yamagata, T. (1999). A dipole mode in the tropical Indian Ocean. *Nature*, *401*(6751), 360–363. https://doi.org/10.1038/43854

Sardeshmukh, P. D., & Hoskins, B. J. (1988). The generation of global rotational flow by steady idealized tropical divergence. *Journal of the Atmospheric Sciences*, *45*(7), 1228–1251. https://doi.org/10.1175/1520-0469(1988)045<1228:tgogrf>2.0.co;2

Seager, R., Cane, M., Henderson, N., Lee, D.-E., Abernathey, R., & Zhang, H. (2019). Strengthening tropical Pacific zonal sea surface temperature gradient consistent with rising greenhouse gases. *Nature Climate Change*, *9*(7), 517–522. https://doi.org/10.1038/s41558-019-0505-x

Seager, R., Henderson, N., & Cane, M. (2022). Persistent discrepancies between observed and modeled trends in the tropical Pacific Ocean. *Journal of Climate*, *35*(14), 4571–4584. https://doi.org/10.1175/jcli-d-21-0648.1

Tippett, M. K., L'Heureux, M. L., Becker, E. J., & Kumar, A. (2020). Excessive momentum and false alarms in late-spring ENSO forecasts. *Geophysical Research Letters*, *47*(8), e2020GL087008. https://doi.org/10.1029/2020gl087008

Williams, N. C., Scaife, A. A., & Screen, J. A. (2023). Underpredicted ENSO teleconnections in seasonal forecasts. *Geophysical Research Letters*, *50*(5), e2022GL101689. https://doi.org/10.1029/2022gl101689

Wu, X., Okumura, Y. M., DiNezio, P. N., Yeager, S. G., & Deser, C. (2022). The equatorial Pacific cold tongue bias in CESM1 and its influence on ENSO forecasts. *Journal of Climate*, *35*(11), 3261–3277. https://doi.org/10.1175/jcli-d-21-0470.1

Zhang, W., Villarini, G., Slater, L., Vecchi, G. A., & Bradley, A. A. (2017). Improved ENSO forecasting using Bayesian updating and the North American multimodel ensemble (NMME). *Journal of Climate*, *30*(22), 9007–9025. https://doi.org/10.1175/jcli-d-17-0073.1

Zhao, Y., Newman, M., Capotondi, A., Di Lorenzo, E., & Sun, D. (2021). Removing the effects of tropical dynamics from North Pacific climate variability. *Journal of Climate*, *34*(23), 9249–9265. https://doi.org/10.1175/jcli-d-21-0344.1